

WIND-INDUCED WATER SURFACE SET-UP AND DRIFT CURRENTS

by

Frederick L.W. Tang¹, Jin Wu², Charles C.C. Chang³,
and Shan-Hwei Ou⁴

ABSTRACT

A systematic experiment to study the wind-induced flow phenomena was conducted in a laboratory tank. The results are related to the wind friction velocity and subsequently scaled for applications at various fetches under different wind velocities. The wind-stress coefficients are found to be well scaled by the Froude number. The bottom friction is measured with an effective shear gauge. The ratios between the bottom stress and the wind stress are obtained. The complete profiles of wind drift current are measured under various wind velocities. A tentative distribution of drift currents in the whole water depth is proposed. The results from the experiment are used to examine the wind-induced flow phenomena in a closed basin.

INTRODUCTION

The water motions induced by wind are involved in many dynamical processes of the mutually-interacting air-sea system. Previous studies on the air-sea interaction, however, seem to concentrate on the atmospheric surface layer and the surface waves. In the past, the wind-induced water-surface set-up and drift currents were measured and analyzed separately. For the surface set-up, it was assumed that the wind stress was balanced by the difference of the hydrostatic pressure due to the surface inclination [Refs. 4 & 7]. Other factors involved were ignored and their influences have not been carefully evaluated. For the drift currents, no systematic experiment has been conducted except for those within the upper layer below the water surface [Refs. 6 & 14]. In the present study, a systematic experiment has been conducted in the wind-wave tank under various wind velocities and wind fetches.

¹ Professor, Dept. of Hydraulic Engineering, National Cheng Kung University, Tainan, Taiwan 700, Republic of China

² Professor, College of Marine Studies and Dept. of Civil Engineering, University of Delaware, Newark, Delaware 19711, U.S.A.

³ Chief Engineer, Taichung Harbour Bureau, Taichung, Taiwan 435, Republic of China

⁴ Visitor, Dept. of Ocean Engineering, University of Hawaii, Honolulu, Hawaii; formerly, Associate Professor, Dept. of Hydraulic Engineering, National Cheng Kung University, Tainan, Taiwan 700, Republic of China

The measurements include the wind profiles, surface waves, surface set-up, current profiles, and bottom friction. All the parameters shown in the free-body diagram of Fig. 1 were measured simultaneously in laboratory wind-wave tank of uniform depth. Various techniques of measurements were illustrated. The results were related to the wind-friction velocity and the wind fetch. The results obtained from all the measurements are substituted into the balancing expression from the free-body diagram; and, the relative importance of each term was also discussed.

EXPERIMENTAL EQUIPMENT AND PROCEDURES

Wind-Wave Tank

Experiments were conducted in the wind-wave tank at the Taichung Harbour Bureau, Taiwan. The tank is 1.5m wide, 2.0m deep and 100m long. Wind is generated by a 75 hp variable-speed fan mounted at the upstream end of the channel. The maximum available wind velocity with a cross section of 0.8m x 1.5m of air passage is above 20 m/s. Wave absorbers were installed at the both ends of the channel to reduce the effect of wave reflection.

Measurements of wind profiles and surface waves were performed at six different fetches: 22^m, 31^m, 37^m, 46^m, 52^m, 58^m and at four different water depths: 1.2^m, 0.9^m, 0.6^m and 0.4^m. Drift current profiles were measured at the fetches of 22^m, 31^m and 37^m, while the bottom frictions were measured only at the middle bottom between fetch 22^m and 31^m.

Fig. 2 is the general outline of the wind-wave tank and the air-water motions. The water motion is assumed to be two-dimensional flow. Select the origin of the axis at the mean water level with x along the channel axis and y vertical and drawn upwards as in Figure 2.

Wind and Wave Measurement Devices

The wind velocities in the channel were measured by pitot-static tube in conjunction with a micromanometer. The tube was supported at the central top of the tank and traversed vertically across the boundary layer of the airflow. The wind velocities were directly read out from the micromanometer.

The surface waves were measured with conductivity probes. The wave signals were recorded on tapes, which were subsequently played back on the analog computer, HP 1000, to determine the wave heights, wave periods, mean water surface elevations and wave spectra. The time interval for the surface data is 0.1 second and the total number of data in each station is 1200.

Current Measurements

Surface drift current was measured by the punched computer cards, 1 cm square saturated with paraffin. The cards were dropped from the channel roof. The surface drift velocities were obtained by timing the

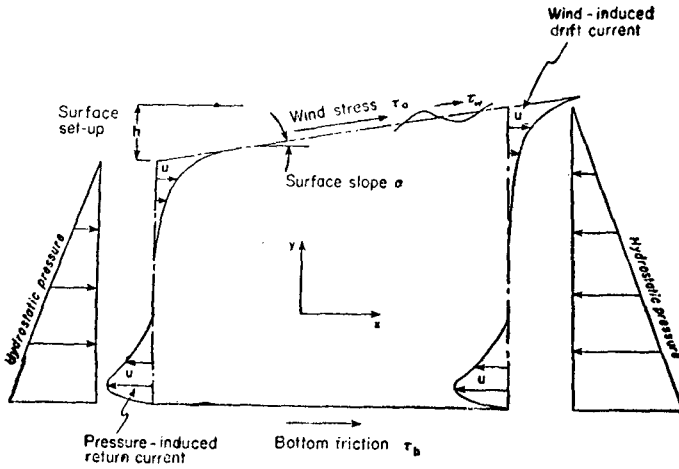


Figure 1. Free-body forces diagram

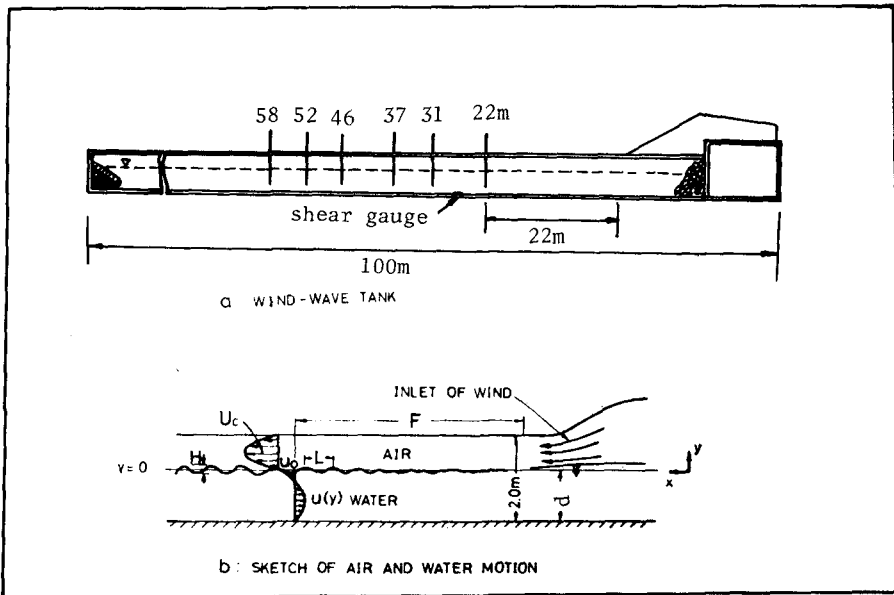


Figure 2. Sketch of wind-wave tank and air-water motions

movements of the cards along a 3m distance. At least five readings were taken for each condition.

The subsurface drift current profiles were measured by dye method. On injecting the dye from the holes on a pvc tube at various elevations, the dye motions were photographed with an 8mm movie camera from the side of the tank. A clear grid was placed outside the channel on the plate-glass sidewall and an electronic clock is placed just below the grid within the camera's view. The dye motion was not laminar, and the velocity flow patterns were confused about ten seconds after the injection of the dye.

The horizontal distances of dye motion at the various depths within time duration were read out from the grid while the time duration was obtained from the electronic clock. The experiments were repeated five to eight times each wind velocity and the average values were taken at the various depths.

Shear Gauge

The shear stress on the tank bottom induced by the return current was measured by a shear gauge, as shown in Figure 3. It consists of three main parts: shear plates, strain gauge, and supported block. The shear plates contain the upper and the lower plate, both 55 cm wide, 65 cm long, and 0.12 cm thick. The lower plate is hung on the supported block by four steel wires (0.5mm diameter) of equal length. The shear plate is sensitive only to the horizontal forces.

The strain gauge is pasted on a steel sheet which is mounted at both ends on the lower plate and the supported block. The steel sheet is carefully adjusted through the screw such that no bending moment is exerted on it when at rest. The shear force acting on the upper plate is transferred to the bending moment on the steel sheet and is recorded on tapes which are then played back on the analog computer. The steel sheet is 0.5mm thick and 7 cm long, which are experimentally examined. The clearance gaps is 1mm along four sides. The shear gauge was statically calibrated.

WIND STRESS AND SCALING CRITERION

The surface set-up and drift currents are governed by the wind stress acting at the air-sea interface. A model scaling criterion for the wind stress coefficient is necessary for the laboratory studies of the field phenomena.

An equation for scaling the wind stress coefficient was given as [Ref. 11]

$$\frac{1}{\sqrt{C_y}} = \frac{1}{k} \ln \left(\frac{1}{0.0112 C_y F_r^2} \right) \quad (1)$$

in which C_y is the wind stress coefficient defined as $C_y = \tau_o / \rho_a U_y^2$; F_r is the Froude number defined as $F_r = U_y / \sqrt{g y}$; k is the Karman's constant;

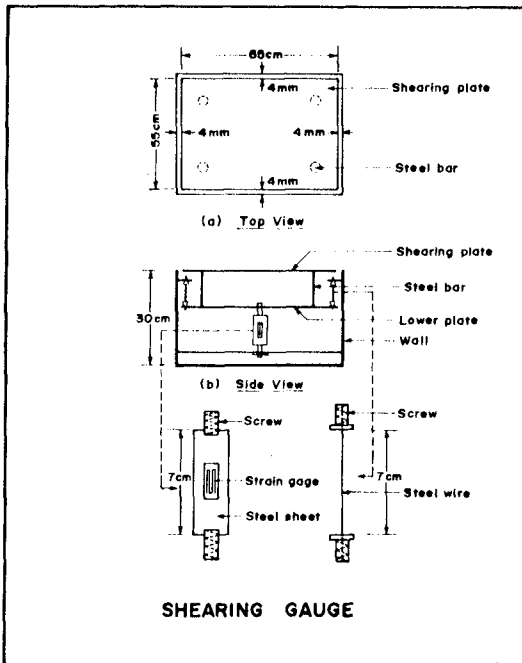


Figure 3. Shear gauge

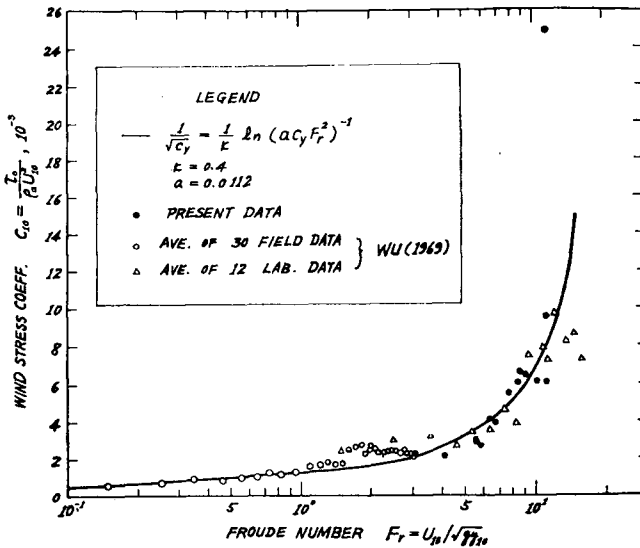


Figure 4. Froude number scaling of wind stress coefficients

and τ_0 is the wind stress, U_y the wind velocity at elevation y , ρ_a the density of air, and g the gravitational acceleration.

This Froude scaling criterion for wind-stress coefficient has been verified by Wu [Ref. 11] with the results of 12 laboratory and 30 oceanic independent data. The present result is given in Figure 4. Good agreement with Froude scaling law was shown.

Since the Froude number scaling law is derived from the logarithmic wind profile [Figure 5], the reference height, y , should be within the inner region of the atmospheric boundary layer. Wu [Ref. 12] proposed the anemometer height in Froude scaling as

$$y = \begin{cases} 10 \text{ cm; for } R < 5 \times 10^7 \\ 7.35 \times 10^{-5} R^{2/3} \text{ cm; for } 5 \times 10^7 < R < 5 \times 10^{10} \\ 10 \text{ m; for } R > 5 \times 10^{10} \end{cases} \quad (2)$$

where R is the fetch Reynold number given as $R = \frac{U_y F}{\nu_a}$, and F denotes the wind fetch, ν_a the kinematic viscosity of air.

Therefore, with a single wind velocity either in the field or in the laboratory at a suggested anemometer height, one can calculate the Froude number, which in turn is given to obtain the wind-stress coefficient. The wind stress and the wind friction velocity can also be obtained.

The dependence of the wind stress coefficient, C_{10} , on fetch was plotted in Figure 6, in which C_{10} indicates the C_y at $y = 10$ cm. In general, C_{10} decreases as F increases for the small wind velocities, while for the high wind velocities, C_{10} decreases first, then increases as F increases. The dependence of the wind friction velocity, U_* , on fetch shows the same tendency as C_{10} does.

BOTTOM FRICTION

The total forces on the test plate before and after the experiment were recorded digitally and analyzed through the analog computer to obtain the mean readings and the time-mean forces. By dividing the area of shear plate, the shear stress was obtained.

Since the bottom friction is oscillatory, the inertial force of the shear plate is involved. An attempt was made to lower reasonably the natural frequency of the steel sheet during the development of the shear gauge.

Figure 7 is the definition sketch of the data in which p indicates the mean reading of oscillatory shear stress after the experiment, q the same reading before the experiment, and A the time-mean range of the force waves. Since the resultant bottom stress is in the same direction as the wind stress [Fig. 1], the average bottom stress, τ_b , is interpreted as $(A/2 + p - q)$, which would correct the inertial force.

The measured values of the average bottom stress were shown in Figure 8 as the function of wind friction velocity. The average bottom stress increases slightly as the wind friction velocity increases. It is also seen that the bottom friction increases remarkably as the water depth decreases. Figure 9 shows the ratio between average bottom stress

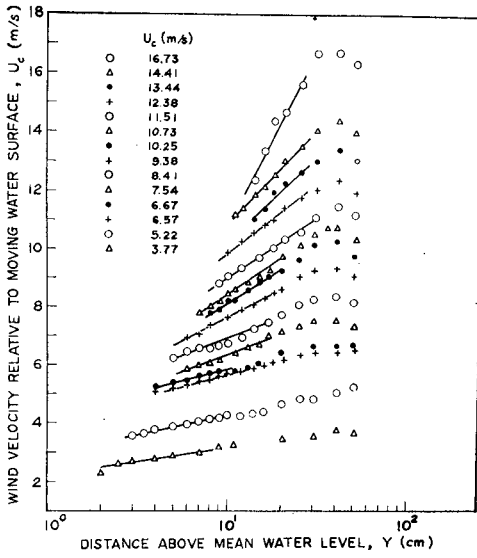


Figure 5. Vertical wind profiles

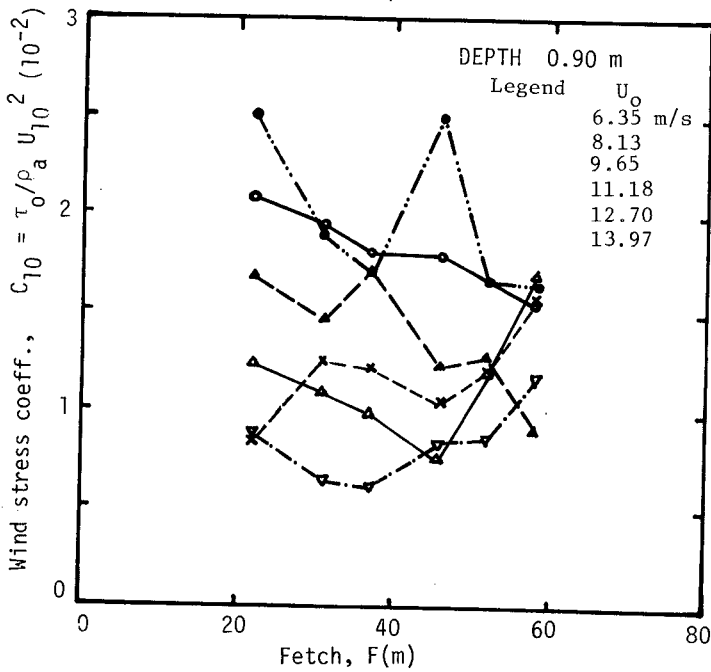


Figure 6. Variation of wind stress coefficient with fetch

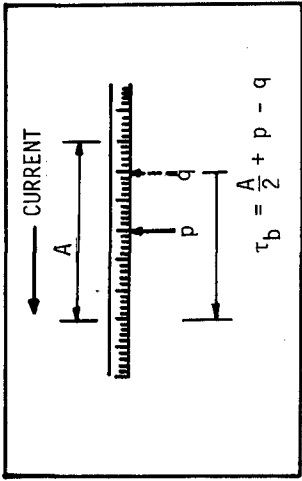


Figure 7. Sketch of data reading of bottom shear

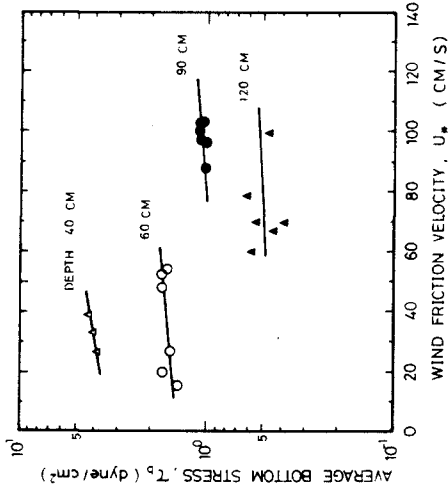


Figure 8. Variation of average bottom stress with wind friction velocity

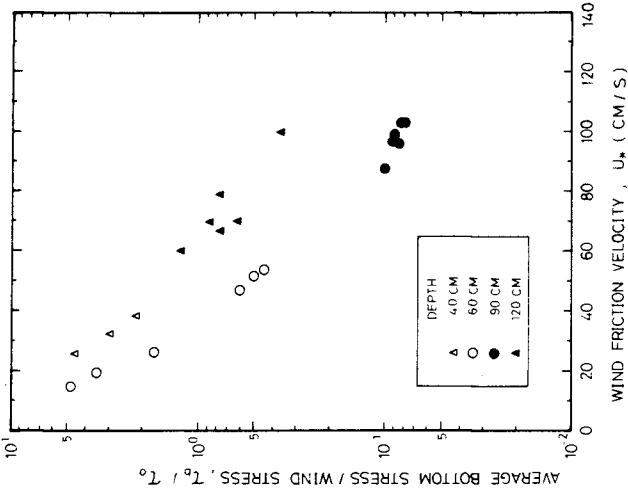


Figure 9. Variation of τ_b/τ_0 with U_*

and wind stress in relation to the wind friction velocity. This ratio has strong dependence on the wind friction velocity, as might be expected because the wind stress is calculated from the square of the wind friction velocity. The measured values of the ratio range from 5 to 0.08 according to the wind velocity and water depth. The value 0.5 assumed by Keulegan [Ref. 4] and 0.1 deduced by Baines & Knapp [Ref. 1] should follow their catalog. This deviation indicates the necessity of measuring rather than calculating the bottom friction when working with a force balance of the free body force diagram.

DRIFT CURRENTS

Surface Drift Currents

The surface drift currents were measured in the plate-glass section of the tank at fetch $F = 31\text{m}$. The measured ratio of the surface drift velocity to the wind velocity was calculated as 0.0311. Table 1 gives the ratio of several sets of experiments in which parts of the wind velocity were referred to the free stream wind velocity.

TABLE 1: Ratio of u_0/U_0

| Author | Method | u_0/U_0 (%) |
|----------------|-------------------|---------------|
| Keulegan | Paraffin particle | 3.3 |
| Tickner | Dye | 3.0 |
| Plate et. al.* | Paper disc | 2.60 |
| Shemdin * | Paper disc | 2.89 |
| Kato et. al. * | Hydrogen bubble | 2.80 |
| Wu | Floats | 3.95 |
| Present data | Paper | 3.11 |

*Wind velocity is referred to as free stream wind velocity

The measured surface drift velocity is plotted in Figure 10 in which Figure (a) shows the variation of u_0 with U_* , Figure (b) shows the variation of u_0/U_* with U_* . The variation of the surface drift with the wind velocity is not fully understood. In this study, the ratio u_0/U_* is around the value of 0.45 at the high wind velocity. It is somewhat lower than the previous results of one of the authors [Ref. 12].

The Stokes transport at the water surface was expressed as [Ref. 2]

$$V_0 = C_0 \left(\frac{\pi H}{L} \right)^2 \quad (3)$$

where H is the wave height, L the wave length, C_0 the phase velocity calculated from Airy wave. The surface Stokes transport is also shown in Figure 10(a).

The wind-induced surface drift is the difference between the total surface drift u_0 and the surface Stokes drift V_0 . This leads to $(u_0 - V_0)/U_* = 0.38$, which is lower than the previous results. This is

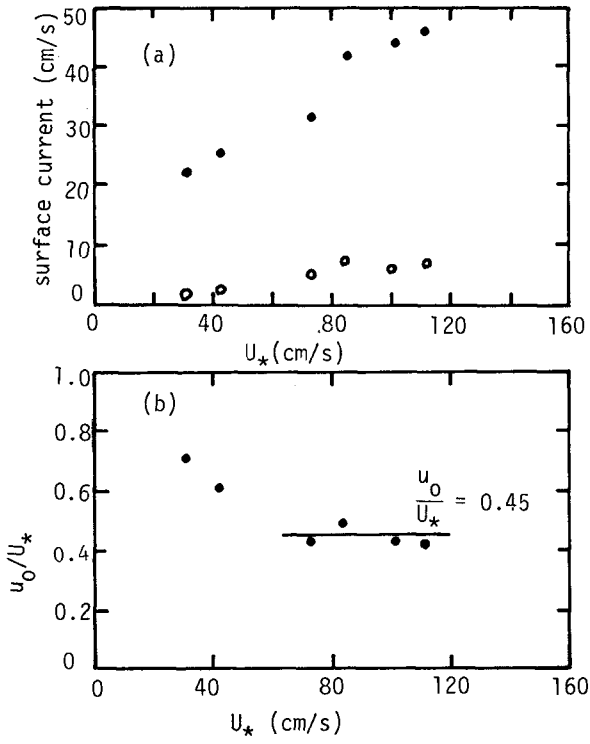


Figure 10. Surface drift velocity for various wind friction velocity
 (Solid: total drift;
 Open : wave-induced)

where more study is needed.

Measurement of Current Profiles

The measurement of the drift current profile is difficult. No complete data have been reported except for Tickner [Ref. 10] and Baines & Knapp [Ref. 1], both of whom made the measurements in shallow water channel at low wind velocities.

Five wind velocities of current profile measurements were conducted in the present study [Ref. 8]. For every wind velocity the profile was worked out from the average of five to eight runs. The current profiles vary with the wind velocity. Five profiles of different velocities were averaged to give the result as the curve E in Figure 11, where previous results are also shown in the figure for comparison.

Curve A in Figure 11 is summarized from the twelve drift current measurements of Wu [Ref. 14] while Curve B is compiled from three profiles of Shemdin [Ref. 6]. The measurements by Wu and Shemdin were aimed at the near surface region. Two curves are very close when y/d is larger than -0.2 , where d denotes the uniform water depth in the tank. Curve C was proposed by Kato [Ref. 3] with the assumption that current velocity at the bottom was equal to that at the half-depth. Curve D was obtained by Tickner [Ref. 10] at the small wind velocities of 3 m/s, in which detergent was added to the water to inhibit the formation of waves.

It is obvious that all of the results show a considerably different shape. In this result, the area under the return current is larger than that under downwind region. The continuity equation of net transport in vertical section is not satisfied. The lateral flow in the channel could cause the inaccuracies.

Analytical Result of Current Profile

Wind stress acting on the water surface causes a forward current in the upper layer and a backward current in the bottom, as shown in Fig. 12. Assuming that the wind stress is steadily and uniformly acting on the water surface, the drift current velocity will change gradually. As a result, the current profile can be separated into two regions: the upper region and the lower region being separated at $y = -\delta$ where $u = u_{\max}$.

The detailed configuration in the upper region is more complicated than the lower region. The wave drag will cause momentum transfer from air to water fluid. However, it is not expected that these effects will penetrate deeply into the fluid. The wind stress exerted on the fluid is like the roughness effect of a boundary. It is convenient to take this flow motion as a semi-pipe flow with the water surface as the pipe-wall. Similarly, the flow in the lower region is taking the flow motion as the semi-pipe flow with the bottom as its pipewall.

Taking the above into consideration, the current profile can be solved as the pipe flow problem. Tang [Ref. 9] solved this turbulent flow by Nikuradse's mixing length formula. The current profiles are given as:

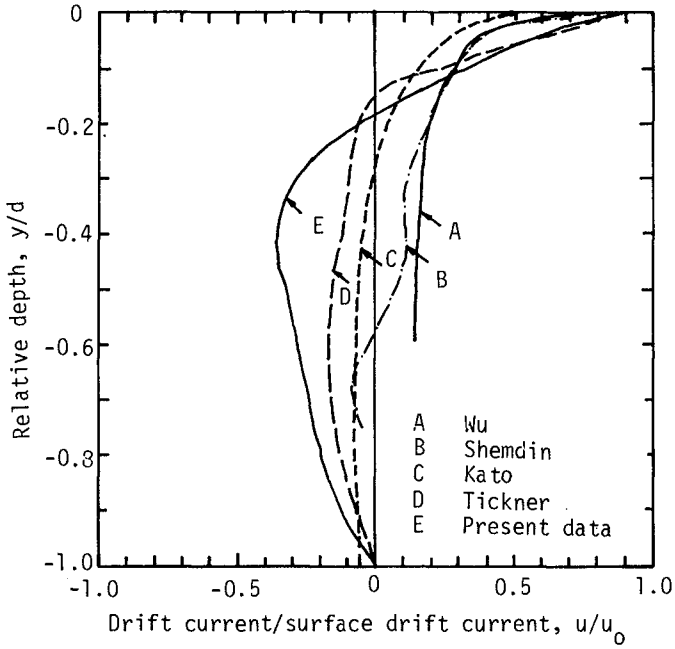


Figure 11. Comparison of drift current profiles

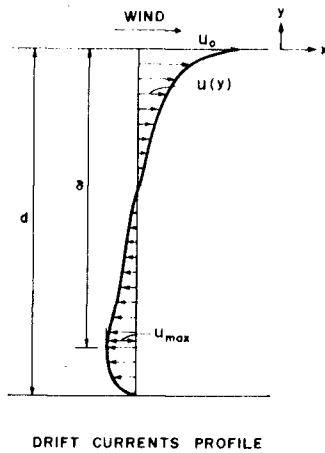


Figure 12. Drift current profile

$$\frac{u_{\max} - u}{u_*} = 2.5 \ln \left(\frac{y}{\delta} \right) + 1.5 \left(\frac{\delta + y}{\delta} \right) - 0.08125 \left(\frac{\delta^2 - y^2}{\delta^2} \right) + 0.06541 \left(\frac{\delta^3 + y^3}{\delta^3} \right) ; \text{ for } -\delta < y < 0 \quad (4)$$

and

$$\frac{u}{nu_*} = 2.5 \frac{d+y+Y}{Y} + 1.5 \left(\frac{d+y}{d-\delta} \right) - 0.08125 \left(\frac{d+y}{d-\delta} \right)^2 + 0.06541 \left(\frac{d+y}{d-\delta} \right)^3 ; \text{ for } -d < y < -\delta \quad (5)$$

where

$$Y = \frac{dn^2}{1+n^2} \exp \left[- \frac{1.760(1+n^3) + 1.484(1-n)}{2.5n(1+n^2)} \right]$$

$$n = \sqrt{\frac{|\tau_b|}{\tau_s}}$$

$$\tau_s = \tau_o - \tau_w$$

u_* = current friction velocity in the upper region

$$\tau_w = \text{wave drag}$$

The computations of Equations (4) and (5) were carried out for cases corresponding to the available experimental results. Good agreement was found, as shown in Figures 13 and 14, with some measured current profiles.

SURFACE SET-UP

The water surface set-up was computed from the data of the surface elevations. The mean water elevation at a station during the test is computed through the computer by sampling the data of surface elevations. The difference between this mean water elevation and the still water level is interpreted as the surface set-up. Surface set-up at the fixed point is sometimes expressed by the surface slope.

Figure 15 shows the relation between the surface slope and the wind friction velocity in the interval of fetches 22^m and 31^m. In general, the surface set-up at the fixed station increases with the increase of wind friction velocity. But the scattered data limit further examination.

The dependence of the surface set-up on the fetch is not clear in this study due to the water oscillation in the tank. Figure 16 gives the relative surface set-up, h/F , as a function of Froude number, including the data from different water depths and different fetches.

The forces exerting on the water body between two sections include the wind stress, bottom friction, momentum flux of drift currents, and hydrostatic pressures at the two sections. For steady condition, the force balance equation can be expressed as

$$\frac{\partial}{\partial x} \int_{-d}^0 \rho_w u^2 dy = -\rho_w g d \tan \alpha + \tau_o + \tau_b \quad (6)$$

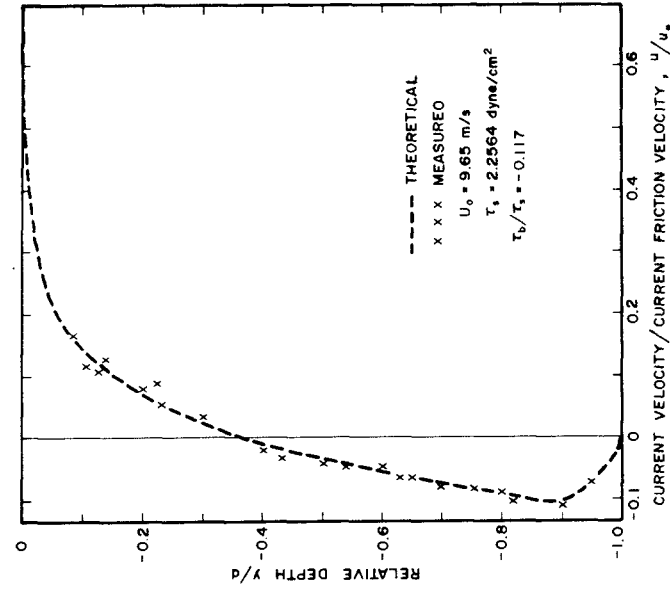


Figure 13. Comparison between proposed current distribution and measured

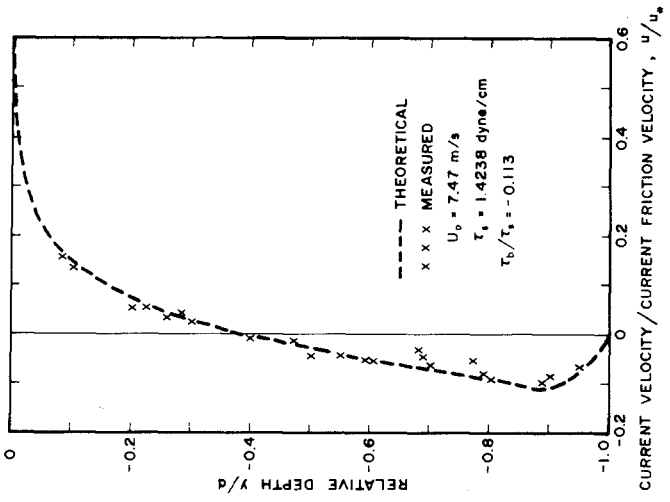


Figure 14. Comparison between proposed current distribution and measured

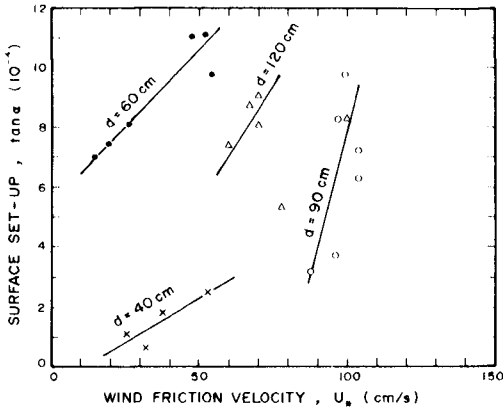


Figure 15. Relation between surface set-up and wind friction velocity at fetch 22^m

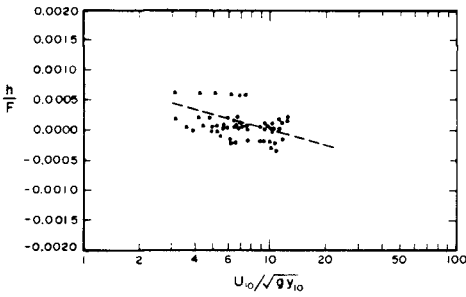


Figure 16. Surface set-up as a function of Froude number

where the left term represents the change of momentum flux due to drift currents and α is the inclination of the water surface between two sections.

Table 2 summarizes the various forces measured at fetch 22^m. If the left term in Equation (6) is neglected, the surface set-up can be estimated as

$$\tan\alpha = \frac{\tau_o + \tau_b}{\rho_w g d} \quad (7)$$

Figure 17 shows the comparison of surface set-up between the measured values and that estimated from Equation (7).

As shown in the figure, the actual water surface set-up is larger than those estimated from the wind stress and bottom friction. In other words, the determination of the wind stress from the water surface slope, which has often been used by the oceanographers, seems to be over-estimated.

TABLE 2: Various Stresses Measured at Fetch 22M

| Depth (cm) | Wind friction velocity U_* (cm/s) | Wind stress τ_o (dyne/cm ²) | Bottom stress τ_b (dyne/cm ²) | Surface set-up $\rho_w g d \tan\alpha$ |
|------------|-------------------------------------|--|--|--|
| 40 | 25.9 | 0.87 | 3.91 | 4.36 |
| | 32.5 | 1.37 | 4.01 | 2.61 |
| | 38.8 | 1.95 | 4.29 | 7.40 |
| 60 | 15.0 | 0.29 | 1.43 | 38.55 |
| | 19.4 | 0.49 | 1.69 | 43.77 |
| | 26.5 | 0.91 | 1.56 | 47.69 |
| | 53.9 | 3.76 | 1.65 | 57.49 |
| | 52.1 | 3.51 | 1.76 | 65.99 |
| | 47.7 | 2.94 | 1.72 | 65.33 |
| 90 | 87.5 | 9.90 | 1.02 | 28.42 |
| | 95.9 | 11.89 | 1.01 | 43.12 |
| | 102.7 | 13.64 | 1.07 | 55.86 |
| | 102.5 | 13.58 | 1.08 | 63.70 |
| | 96.7 | 12.09 | 1.10 | 73.50 |
| | 99.4 | 12.78 | 1.11 | 86.24 |

CONCLUSIONS

An attempt has been made for a systematic experiment covering all the dynamical forces on the water free body. Main findings are as follow:

1. Froude scaling criterion for the wind stress coefficient is confirmed, enabling the present results to be scaled for general application.
2. The bottom friction increases slightly with the increase of wind friction velocity, while the ratio between the bottom stress and the wind

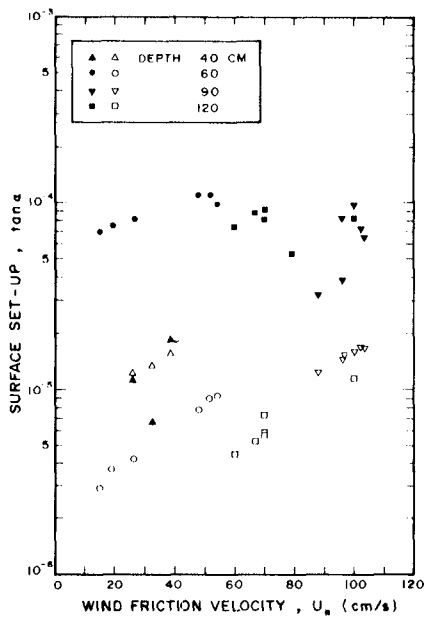


Figure 17. Surface set-up from measured and estimated
 (Solid: measured
 Open : estimated)

stress decreases rapidly with the increase of wind velocity.

3. A complete distribution of the mean current velocity is proposed for prediction of drift currents.

4. The wind stress determined from the inclination of the mean water surface is found to be larger than that obtained from the wind profiles.

ACKNOWLEDGEMENTS

This work was supported by both the National Science Council, Republic of China (Contract No. NSC 66-0501-0202(-17)), and the National Science Foundation, United States of America (Grant No. NSF OIP 75-15806).

REFERENCES

1. Baines, W.D. and D.J. Knapp (1965): Wind driven water currents, J. Hydraulics Division, ASCE 91, p. 205-221.
2. Chang, M.S. (1969): Mass transport in deep-water, longcrested random gravity waves, J. Geophysics Res. 74, p. 1515-1536.
3. Kato, H. (1974): Calculation of the wave speed for a logarithmic drift current, Rept. Port and Harbour Research Inst. 13, No. 4, p. 4-32.
4. Keulegan, G.H. (1951): Wind tides in small closed channels, Journal Res. National Bureau Standards 46, p. 358-381.
5. Plate, E.J., P.C. Chang and G.M. Hidy (1969): Experiments on the generation of small water waves by wind, J. Fluid Mechanics 35, p. 625-656.
6. Shemdin, O.H. (1972): Wind-generated current and phase speed of wind waves, J. Physical Oceanogr. 2, p. 411-419.
7. Sibul, O.J. and J.W. Johnson (1959): Laboratory study of wind tides in shallow water, J. Waterways and Harbour Division, ASCE 97, WW1, p. 1210-1 to 1210-32.
8. Tang, F.L.W., S.H. Ou, C.C.C. Kao, J. Wu, C.C.C. Chang (1977): Wind-induced water surface set-up and drift currents (I), Proc. First Conf. on Ocean Engineering, Taipei, Taiwan, p. 165-189.
9. Tang, S.Y. (1977): Research on velocity profile of wind drift current, MS Thesis under supervision of F.L.W. Tang, National Taiwan University, Republic of China.
10. Tickner, E.G. (1961): Transient wind tides in shallow water, TM-123, U.S. Army Corps of Engineers, Beach Erosion Board, Washington, D.C.
11. Wu, J. (1969): Froude number scaling of wind stress coefficients, J. Atmospheric Science 26, p. 408-413.
12. Wu, J. (1971): Anemometer height in Froude scaling of wind stress, J. Waterways, Harbors and Coastal Engineering Div., ASCE 97, WW1, p. 131-137.
13. Wu, J. (1973): Prediction of near-surface drift currents from wind velocity, J. Hydraulics Division, ASCE 99, p. 1291-1302.
14. Wu, J. (1975): Wind-induced drift currents, Journal of Fluid Mechanics 68, p. 49-70.